

Rapid identification of time-frequency domain gravitational wave signals from binary black holes using deep learning

Yu-Xin Wang¹, Shang-Jie Jin¹, Tian-Yang Sun¹, Jing-Fei Zhang¹, and Xin Zhang^{1,2,3*}

¹ *Key Laboratory of Cosmology and Astrophysics (Liaoning) & College of Sciences,
Northeastern University, Shenyang 110819, China*

² *Key Laboratory of Data Analytics and Optimization
for Smart Industry (Ministry of Education),
Northeastern University, Shenyang 110819, China*

³ *National Frontiers Science Center for Industrial Intelligence and Systems Optimization,
Northeastern University, Shenyang 110819, China*

Abstract

Recent developments in deep learning techniques have offered an alternative and complementary approach to traditional matched filtering methods for the identification of gravitational wave (GW) signals. The rapid and accurate identification of GW signals is crucial for the progress of GW physics and multi-messenger astronomy, particularly in light of the upcoming fourth and fifth observing runs of LIGO-Virgo-KAGRA. In this work, we use the 2D U-Net algorithm to identify the time-frequency domain GW signals from stellar-mass binary black hole (BBH) mergers. We simulate BBH mergers with component masses from 5 to 80 M_{\odot} and account for the LIGO detector noise. We find that the GW events in the first and second observation runs could all be clearly and rapidly identified. For the third observing run, about 80% GW events could be identified. In particular, GW190814, currently unknown, is a special case that can be identified by the network, while other binary neutron star mergers and neutron star-black hole mergers can not be identified. Compared to the traditional convolutional neural network, the U-Net algorithm can output the time-frequency domain signal images rather than probabilities, providing a more intuitive investigation. Moreover, some of the results through U-Net can provide preliminary inference on the chirp mass information. In conclusion, the U-Net algorithm can rapidly identify the time-frequency domain GW signals from BBH mergers and potentially be helpful for future parameter inferences.

*Corresponding author; Electronic address: zhangxin@mail.neu.edu.cn

Contents

I. Introduction	2
II. Methodology	5
A. Dataset assembly	5
B. U-Net architecture	7
C. Training	9
III. Results and discussion	12
A. Simulation results	12
B. Robustness test of U-Net	14
C. Application to the real observations	16
IV. Conclusion	19
Acknowledgments	20
References	20
A. Results of U-Net	33

I. INTRODUCTION

In 2015, the first detection of a gravitational wave (GW) signal GW150914 from a binary black hole (BBH) merger initiated the new era of GW astronomy [1]. Moreover, it also provided an important test for the existence of GW, which was predicted by Albert Einstein in 1916 based on his general relativity [2]. On August 17th, 2017, the first detection of a binary neutron star (BNS) merger event GW170817 [3], together with its electromagnetic (EM) counterparts, opened the era of multi-messenger astronomy [4]. So far, the LIGO-Virgo-KAGRA collaboration [5–7] has detected 90 GW events from compact binary coalescences (CBCs) [8–12]. The study of GW has important applications in fundamental physics, astronomy, and cosmology. For example, GWs could be used to test general relativity [13–20], understand the origins and distributions of astrophysical CBC sources [21–24], and measure cosmological parameters [25–30] (especially for providing an independent mea-

surement of the Hubble constant using the standard siren method, which is widely discussed in the literature [31–78]).

The traditional matched filtering techniques have achieved great success in the detection of GWs in the past years [79] and the performance of the matched filtering technique is considered optimal. Searches with two different latencies are performed: online and offline searches, as described in Ref. [80]. Online searches are performed in near real-time during the data collection process, while offline searches are conducted later using the final, calibrated, and cleaned dataset. Online analysis allows for the rapid release of candidate-related public alerts for searching multi-messenger counterparts. Offline analysis includes improved background statistics and extensive data calibration, review, and adjustment. At the same time, with relaxed latency requirements, offline analysis can perform more computationally expensive calculations to enhance the ability to separate signals from the background noise. Due to these factors, offline analysis is more sensitive than online analysis. Online searches are rapid, but the ability to separate signals from the background noise are not as strong as offline searches. Furthermore, both of these searches demand substantial computational resources. Nevertheless, deep learning can serve as a complementary approach to validate results generated by the low-latency workflow. In addition, because of the generalization of deep learning [81], deep learning is hopeful to identify the GW signals beyond the GW template, which is expected to be verified by future GW templates. More importantly, deep learning is known for its low computational resource requirements.

Deep learning is a class of algorithms for machine learning. The basic principle of deep learning is to use a multi-layer neural network to gradually extract features from the original input data and make predictions. Thanks to the rapid development of graphics processing unit technology, deep learning techniques have gradually been widely used in various fields in recent years [82–85]. The main advantage of using deep learning to identify GW signals is that the algorithm can be pre-trained using a library of known waveform templates and detector noise. When running an online search, the trained network can be quickly loaded, allowing rapid and efficient identification of GW sources.

Recently, GW astronomy based on deep learning algorithms has been intensively discussed in the literature [81, 86–121]. Among them, Refs. [81, 103–121] focused on the identification of GW signals, and most works were based on the time domain analysis. In fact, because the signal strength characteristic of GW is weak, it would be sub-optimal to

use 2D data in the analysis of GW detection [103]. However, many networks work better with 2D images. To get a higher true alarm rate, and a lower false alarm rate, we conduct analysis in the time-frequency domain. Therefore, the identification of time-frequency domain analysis of GW based on deep learning is also very important, which is discussed in Refs. [90, 122–124]. The 2D U-Net algorithm [125] has advantages in image processing, which performs quite well in removing foreground contaminations entangled with radio telescope’s systematic effects in neutral hydrogen 21 cm intensity mapping survey [126, 127]. Given the advantage of U-Net in image processing and the similar challenges of identifying the extremely faint neutral hydrogen signals and distinguishing GW signals from noise (GW detection and neutral hydrogen 21 cm intensity mapping survey both extract weak signals from strong background noise), it naturally motivates us to explore the potential of the 2D U-Net algorithm in identifying time-frequency domain GW signals from BBHs.

In this work, we wish to explore the potential of the U-Net algorithm to identify the GW signals. Different from the traditional convolutional neural network (CNN) algorithm, the U-Net algorithm can output images rather than probabilities, enabling a more intuitive investigation from the time-frequency domain signal. Our goal is to train the network that can directly output the GW signal image in the time-frequency domain. Given that the currently detected GW signals are mainly BBH mergers, we focus on the identifications of BBH mergers. We begin by training the network using simulated BBH signals and subsequently apply the trained network to real observations. Moreover, this is the first work to perform time-frequency domain analysis and apply the network to the O3 observations. Through this work, we aim to shed light on the possibility of using U-Net to identify the GW signals from the BBH mergers. As for the BNS and neutron star–black hole (NSBH) mergers, we leave for our future work.

This work is organized as follows. In Sec. II, we introduce the methodology used in this work. In Sec. III, we report the identification results of the trained network in the simulation data and the O1, O2, and O3 data. The conclusion is given in Sec. IV.

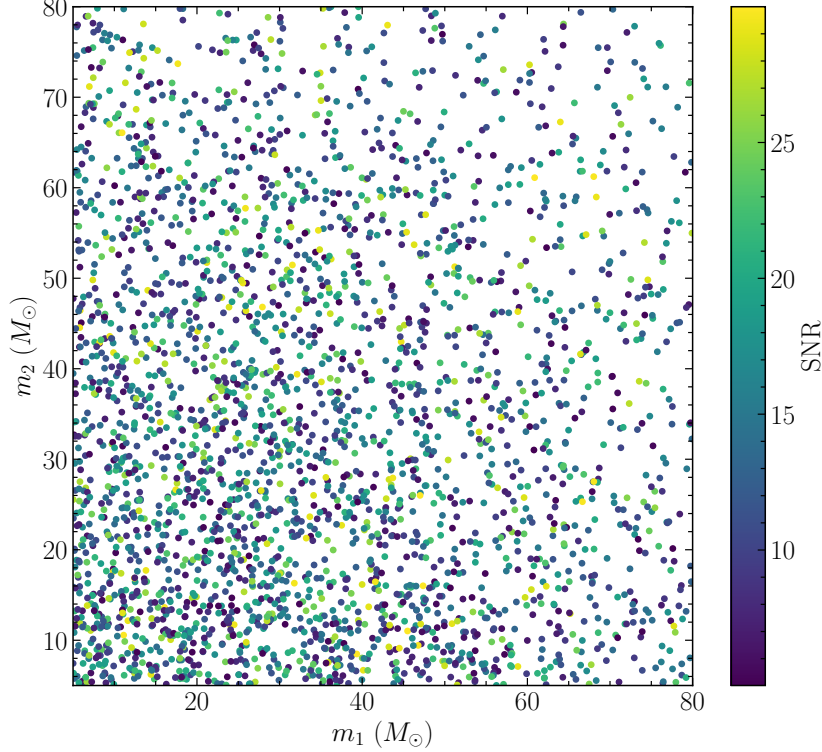


FIG. 1: Single mass (m_1, m_2) and SNR of the training data. Note that we show only 3/20 data for simplicity.

II. METHODOLOGY

A. Dataset assembly

In this work, we focus on the GW signals produced by BBH mergers. We generate two datasets of 20000 samples each for training. One is the dataset of pure background noise and the other is the dataset of GW signal and background noise. For the simulated GW signal, we adopt the numerical relativity waveform SEOBNRv4_{opt} [128] (an optimized version of SEOBNRv4 [129]) generated by PyCBC [130]. For the background noise, we select segments of data from the publicly available O1, O2, and O3 data where no GW events were detected. The synthetic data can be written as

$$s(t) = h(t) + n(t), \quad (1)$$

where $h(t)$ is the GW signal and $n(t)$ is the background noise.

The duration of the training dataset is 8 s (we set the merger-time range for the GW

signal to $[6.75, 7.25]$ s) and the sampling rate is 4096 Hz. All the data are whitened and passed through a pass filter with a frequency in the range of $[30, 900]$ Hz. Due to the edge effect of the pass filter, for the data in the edge 0.25 s, we set the data to zero. Subsequently, we utilize the short-time Fourier transform and apply a Hanning window to transform the signals into the time-frequency domain for analysis. Specifically, the window length is set to 0.1 s and the overlap is half the window length. We preprocess our data to fit the network's required dimensions, setting both the time and frequency bins to 160. Subsequently, we apply maximum normalization to each image through dividing all pixel values by the image's highest pixel value, ensuring the maximum pixel value in each image is normalized to 1.

The simulated GW parameters are shown in Table I. Note that the distance is a fixed value, but we rescale the simulated waveform to match SNR, which is randomly chosen in the range of $[5, 30]$, shown in Fig. 1. For the same SNR, the smaller-mass BBHs produce smaller strains, and thus they are difficult to identify. In order to improve the ability of the network to identify signals within the insensitive ranges, we train the network with more low-mass signals (the number of $5 M_{\odot}$ is 5 times more than $80 M_{\odot}$). For SNR, we also adopt the same treatment, we train the network with more low-SNR signals (the number of $\text{SNR} = 5$ is 5 times more than $\text{SNR} = 30$).

Here we emphasize that the detections of BNS mergers are also important, particularly for the observations of the follow-up electromagnetic counterparts, which could greatly advance the fields of multi-messenger astronomy and the standard siren cosmology. In this work, we only consider the BBH mergers for two reasons. First, in order to ensure the robustness of the algorithm, we need as many verification sets as possible. Given that the current detected CBCs by LIGO-Virgo-KAGRA are mainly BBH mergers, they serve as suitable candidates for testing and validating our methods. Second, due to the extended duration of BNS merger detections compared to BBH mergers, the data dimension is relatively high. Without employing PCA for dimensionality reduction, the dataset requirements would experience exponential growth. Consequently, BNS mergers should be treated with dedicated networks and separately with BBH [116, 131].

TABLE I: Distribution of simulated GW waveform parameters. Note that other parameters not mentioned are set to zero for simplicity.

Parameter	Uniform distribution
Component masses	$m_1, m_2 \in [5, 80] M_\odot$
Right ascension	$\varphi \in [0, 2\pi]$
Declination	$\theta \in [-\pi/2, \pi/2]$
Polarization angle	$\psi \in [0, 2\pi]$
Injection SNR	$\text{SNR} \in [5, 30]$

B. U-Net architecture

The typical use of convolutional networks is on classification tasks, where the output of the image is a single class label. However, in many visual tasks, it is not enough to assign a single class label to an entire image. Instead, the desired output should include pixel-level localization, where a class label is assigned to each individual pixel. The U-Net algorithm can achieve this through semantic segmentation, which is an approach for identifying the class of an object for each pixel. The approach is particularly useful for tasks such as object detection, where the precise location and shape of the object of interest need to be identified.

The U-Net network is a CNN originally developed for biomedical image segmentation [125]. While based on CNN, it has undergone significant structural modifications. Unlike the standard CNN architecture, U-Net includes many feature channels in the upsampling part,¹ allowing the network to propagate contextual information to higher resolution layers through a series of transpose convolutions.² The main idea behind U-Net is to add successive

¹ It refers to any technique that allows an image to be changed to a higher resolution. The simplest way is resampling and interpolating: rescale the input image to a desired size, count the pixels at each point, and use interpolation methods such as bilinear interpolation to interpolate the remaining points to complete the upsampling process.

² Each convolutional layer is composed of a specified number of kernels. Each kernel multiplies the input feature values with weights and adds the biases to obtain outputs. Different kernels get different parameter values after training.

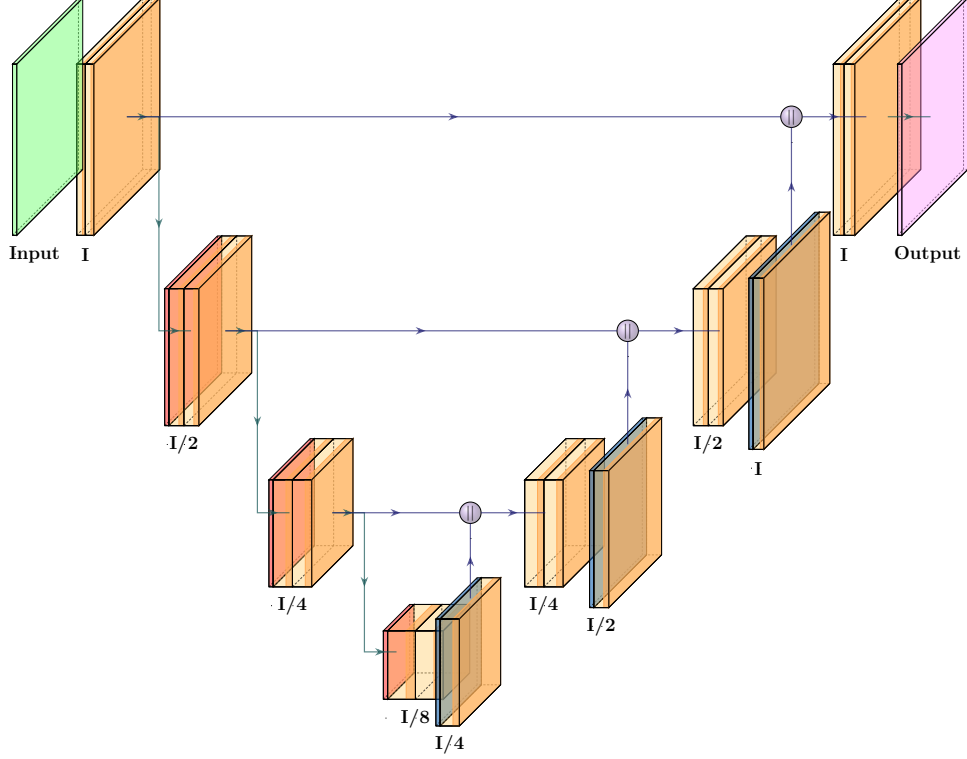


FIG. 2: The training process of CNN with U-Net architecture. Here each color represents a structure in the U-Net network, where yellow cubes represent the convolutional layers and ReLU sections, red cubes represent pooling layers in down-sampling, blue cubes represent the transposed convolutional layers, and grey cubes represent connection layers. The visualization is made with the PlotNeuralNet library [132].

layers to the traditional contracting network, replacing the convergence operation with an upsampling operation. This leads to an increase in output resolution, as these layers produce a U-shaped structure that is almost symmetric with the contracted part.

The network architecture is illustrated in Fig. 2. It consists of a contracted path (left side) and an extended path (right side). The contracting path follows the typical architecture of a convolutional network. It consists of the repeated application of a 3×3 convolutions (unpadded convolutions), each followed by a rectified linear unit (ReLU) and a 2×2 max pooling³ operation with stride 2 for downsampling. At each downsampling step, we double the number of feature channels. Every step in the expansive path consists of an upsampling

³ This layer scans the data according to a specified stride within a window of a certain length. Then, it outputs the maximum value of the data in each scanning window.

of the feature map followed by a 2×2 convolution that halves the number of feature channels, a concatenation with the corresponding cropped feature map from the contracting path, and two 3×3 convolutions, each followed by a ReLU. The cropping is necessary due to the loss of border pixels in every convolution. At the final layer, a 1×1 convolution is used to map each 64-component feature vector to the desired number of classes. In total, the network has 3 convolutional layers.

The flowchart of network is shown in Fig. 3. Whenever a time-frequency domain image is sent to the network, it outputs a noise-reduced image. If the image includes a GW signal, the signal will be highlighted; otherwise, the image will appear almost blank, with pixel values close to zero, rather than exactly zero. For large test datasets, we analyze by extracting the maximum pixel value from each image and comparing it with a predetermined threshold. Images with maximum values exceeding this threshold are considered to contain a GW signal, whereas those below are deemed signal-free.

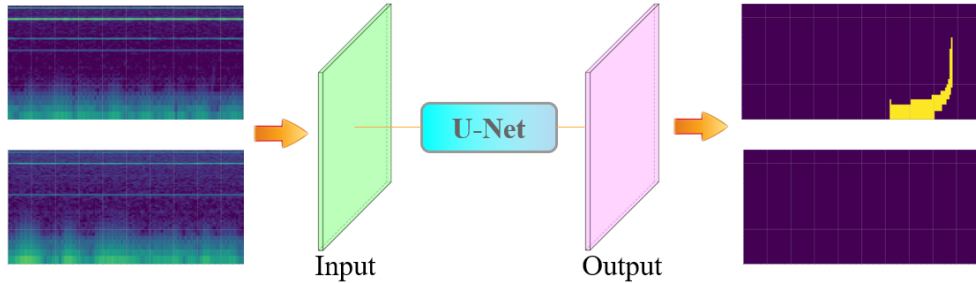


FIG. 3: Flowchart of network used in this work. The observed signal [133] (GW signal+noise or noise only) is processed by the U-Net algorithm. If the GW signal is present, the GW signal image will be outputted. If there is no signal, an empty signal image will be outputted.

C. Training

During the training process, the coefficients of the neural network are determined. To assign initial random values to the CNN parameters, we use the “Xavier” initialization, which is designed to keep the scale of gradients roughly the same in all layers. Then, we use the binary cross-entropy loss function to evaluate the deviation between the predicted values and the actual values in the training data.

The key component of CNN is the convolutional layer, which applies a set of filters to the

TABLE II: Description of the hyperparameters in the U-Net architecture design.

Hyperparameter	Description	Prior value	Optimum value
η	learning rate for optimizer	$10^{-3}, 10^{-4}, 10^{-5}, 10^{-6}$	10^{-5}
ω	weight decay for optimizer	$10^{-4}, 10^{-5}, 10^{-6}, 10^{-7}$	10^{-5}
n_{filter}	initial number of convolution filters	16, 32	32
b	batch size	32, 64	32
Ω	optimizer for training	Adam, NAdam	NAdam

input. The network consists of a series of stacked layers. In the first convolutional layer, we set the number of convolution kernels to 32. The kernel size determines the convolutional field of view and is fixed at 3×3 . To maintain the output dimensionality, we employ the same padding method for both convolutions and transpose convolutions to handle sample boundaries. The stride determines the kernel traversal step size on the images. We use the default stride settings of 1 in convolutions and 2 in transpose convolutions.

Our selected U-Net architecture is trained end-to-end to the signal identification using the simulated data introduced in Sec. II A. The details of the hyperparameters used in this work are listed in Table II. The prior value is the value we used during the training process which can get a high true alarm rate with a threshold to be 0.5, and the optimum value is the value we finally selected which has the best ROC. The NAdam optimizer⁴ is used in the analysis with the default TensorFlow parameters [134]. The hyperparameters are carefully fine-tuned to optimize the network. The batch size is optimized to 32 and the number of initial convolution filters is optimized to 32, both of which are limited by the GPU memory. The learning rate⁵ is set to 10^{-5} , and weight decay is 10^{-4} . We set dropout to be 0.2 and

⁴ In the process of deep learning backpropagation, the optimizer guides each parameter of the loss function (objective function) to update the appropriate size in the right direction, so that the updated parameters make the value of the loss function (objective function) approach the global minimum continuously.

⁵ In machine learning and statistics, the learning rate is a tuning parameter in an optimization algorithm that determines the step size at each iteration while moving toward a minimum loss function.

TABLE III: GW events that are not considered in this work.

Name	Event type
GW170817	BNS
GW190425	BNS
GW190814	NSBH
GW190917_114630	NSBH
GW191219_163120	NSBH
GW200105_162426	NSBH
GW200115_042309	NSBH
GW200210_092254	NSBH

use batch normalization⁶ to make the mean and variance of the input data distribution of each layer in U-Net within a certain range. The total number of trainable parameters is 3.1×10^6 . We apply a ReLU activation in every convolution. At last, we adopt the 200 epoch calculation scheme to improve our results.

At the end of every epoch, the performance of the network during the training is evaluated by average accuracy for the networks on each mini-batch. The training process is done within 6 hours on 4 NVIDIA GeForce RTX A6000 GPUs, each with 48 GB of memory.

The identification times for 173 GW signals⁷ is 0.1868 s, meaning that the identification time for each GW signal is about 1 ms. On the other hand, compared to the matched filtering method, U-Net can save computation resources.

⁶ In the training process of each batch after the data passes through the activation layer, the activation value of each batch of data is normalized. In other words, the average value of the sample data of each batch is normalized to 0 and the variance is normalized to 1. The purpose of this step is to make the result of batch normalization the same as the original input data, which maintains the possibility of retaining the original structure.

⁷ Note that we consider the GW signals from both LIGO Hanford and LIGO Livingston. We consider 86 GW signals for LIGO Hanford and 87 signals for LIGO Livingston.

III. RESULTS AND DISCUSSION

A. Simulation results

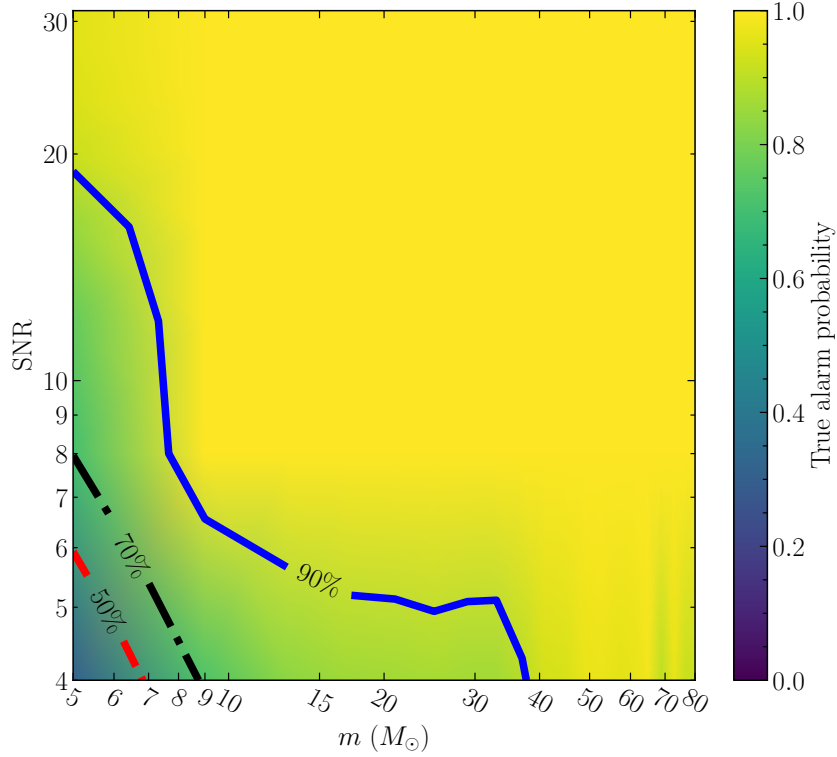


FIG. 4: Network robustness on m with respect to SNR. Note that we consider the equal-mass BBH mergers.

We first study the ability of the network in GW detections considering the single mass m and SNR. In the training dataset, we consider the equal-mass BBH mergers, the BH mass is sampled in the range of $[5, 80] M_\odot$, and SNR is sampled in the range of $[5, 30]$. After 100 epochs of training, the accuracy of the test dataset is 90%. In order to show the ability of the network, we show the results in Fig. 4 with m and SNR in the ranges of $[5, 80] M_\odot$ and $[4, 32]$, respectively. We find that the network performs well in the high-mass and high-SNR regions, but not well in the low-mass and low-SNR regions. Therefore, for the lower-SNR region ($4 < \text{SNR} < 5$), the network also performs not well. The prime cause is that the network is more effective for handing short signals. As the mass decreases, the GW signals last longer and become buried within the characteristics of the random noise. In other words, because SNR is integrated throughout the GW signals, at the same SNR, short signals have

TABLE IV: Testing the robustness of networks to GW signals added to noise at different times .

Time (s)	True alarm probability
6.75	0.9840
6.90	0.9880
7.00	0.9910
7.10	0.9884
7.25	0.9754

higher strain values than those of long signals. Therefore, it is easier to identify the short signals. For the high-mass and low-SNR regions, the network performs better. Concretely, the network performs well when the single mass is higher than $9 M_{\odot}$ and SNR is greater than 8.

We second test the robustness of networks where GW signals are added to noise at different times. We select several fixed signal added times [6.75, 6.9, 7, 7.1, 7.25] s to test whether the network can identify signals with different added times. We generate nearly 20,000 samples. The true alarm probability is shown in Table IV. We use the maximum pixel value in the image predicted by the network to compare with a threshold which is set to 0.5. We also generate nearly 20,000 pure noise samples and the false alarm probability is 0.0038.

By training the network with the LIGO noise data in O1, O2, and O3, we use the test dataset for the final evaluation of the network. In Fig. 5, we show the receiver operating characteristic (ROC) curve, which illustrates the diagnostic ability of a binary classifier system [135]. When the discrimination threshold changes, the ROC curve reflects the proportion of positive samples correctly identified (True alarm probability) versus the proportion of negative samples incorrectly identified (False alarm probability) [136]. In this work, when the true alarm probability of O3 test data exceeds 0.94, the threshold is 0.51. In addition, the false alarm probability of the network is better than 0.1%, which is comparable with the network in the recent literature [113, 115, 137].

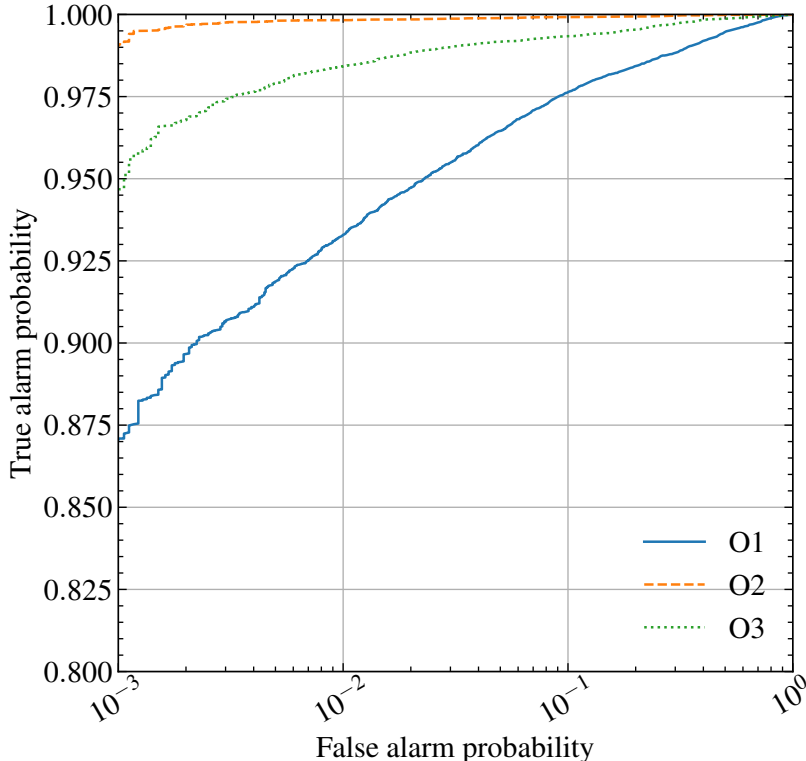


FIG. 5: Receiver operating characteristic (ROC) curve of the network trained by the LIGO noise data in O1, O2, and O3.

B. Robustness test of U-Net

In the process of identifying GW signals, as a typical non-stationary noise for GW detectors, glitches often have a great impact on the matched filtering method. Glitches may also have an impact on the false alarm rate of U-Net. Hence, in this subsection, we test the impact of the glitches on the false alarm rate of the network which is not trained on glitches before.

We choose the blip glitches as the representative of the glitches. Blip glitches are very short-duration transients ($\mathcal{O}(10)$ ms) and have a wide frequency bandwidth ($\mathcal{O}(100)$ Hz) [138]. We choose the blip glitches for two reasons, (i) the blip glitches is common in the GW data, and (ii) the blip glitches in the time-frequency domain is similar to the high-mass BBH mergers, and thus it can be mistaken for a real GW signal [138, 139].

We used the trained network to identify the blip glitches. Concretely, we chose the blip-

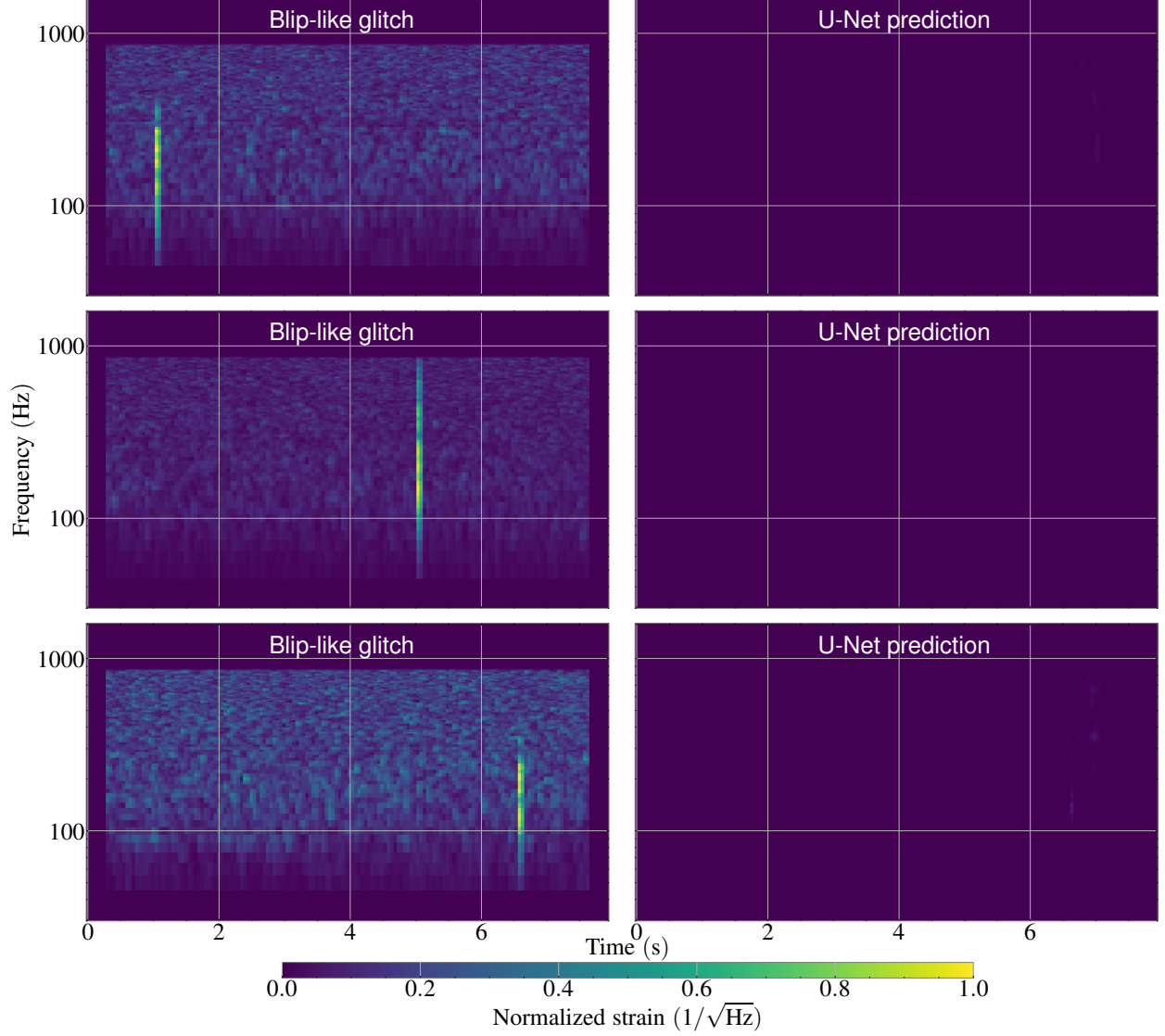


FIG. 6: Blip-like glitches at different times (left panels) and the prediction results of U-Net (right panels).

like glitches from the LIGO data. Then we placed the glitches at different times and used the trained network to identify them. As mentioned above, if the network does not identify the signal, an empty signal image will be outputted. We randomly tested 200 glitches and 6 glitches were identified as signals. In other words, the false alarm rate is about 3% for the blip-like glitch. In Fig. 6, we show three typical blip-like glitches at different times and the prediction results of U-Net. The blip glitches are relatively similar to the waveform of GW at the merge-time, and both resemble the shape of a chirp signal. This might be the reason behind the high false alarm rate.

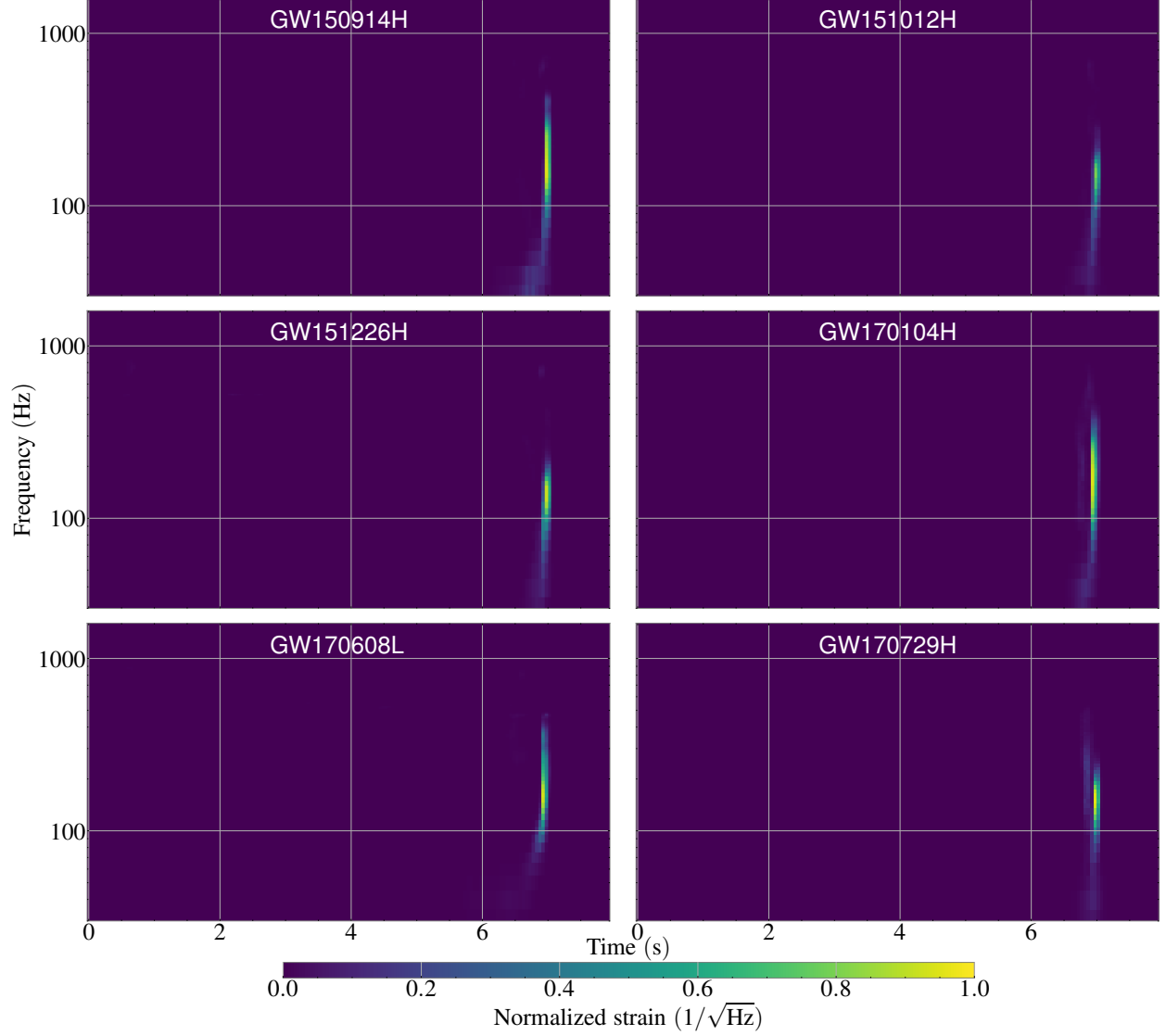


FIG. 7: The time-frequency representation of GW signals of O1 and a portion of O2 identified by the trained network, with the remaining O2 signals presented in Appendix A. In the event names, H and L represent the signals from LIGO Hanford and LIGO Livingston, respectively.

C. Application to the real observations

We apply the trained network to the O1 and O2 data. In this subsection, we shall report the identification results. We test the real GW events by placing the signal around 7 s to make it easier to confirm the results. For each GW event, we identify the GW signals from LIGO Hanford and LIGO Livingston. Due to the low SNR of some GW signals, there will be missed detections during identification. Hence, we adopt the form of the union of LIGO

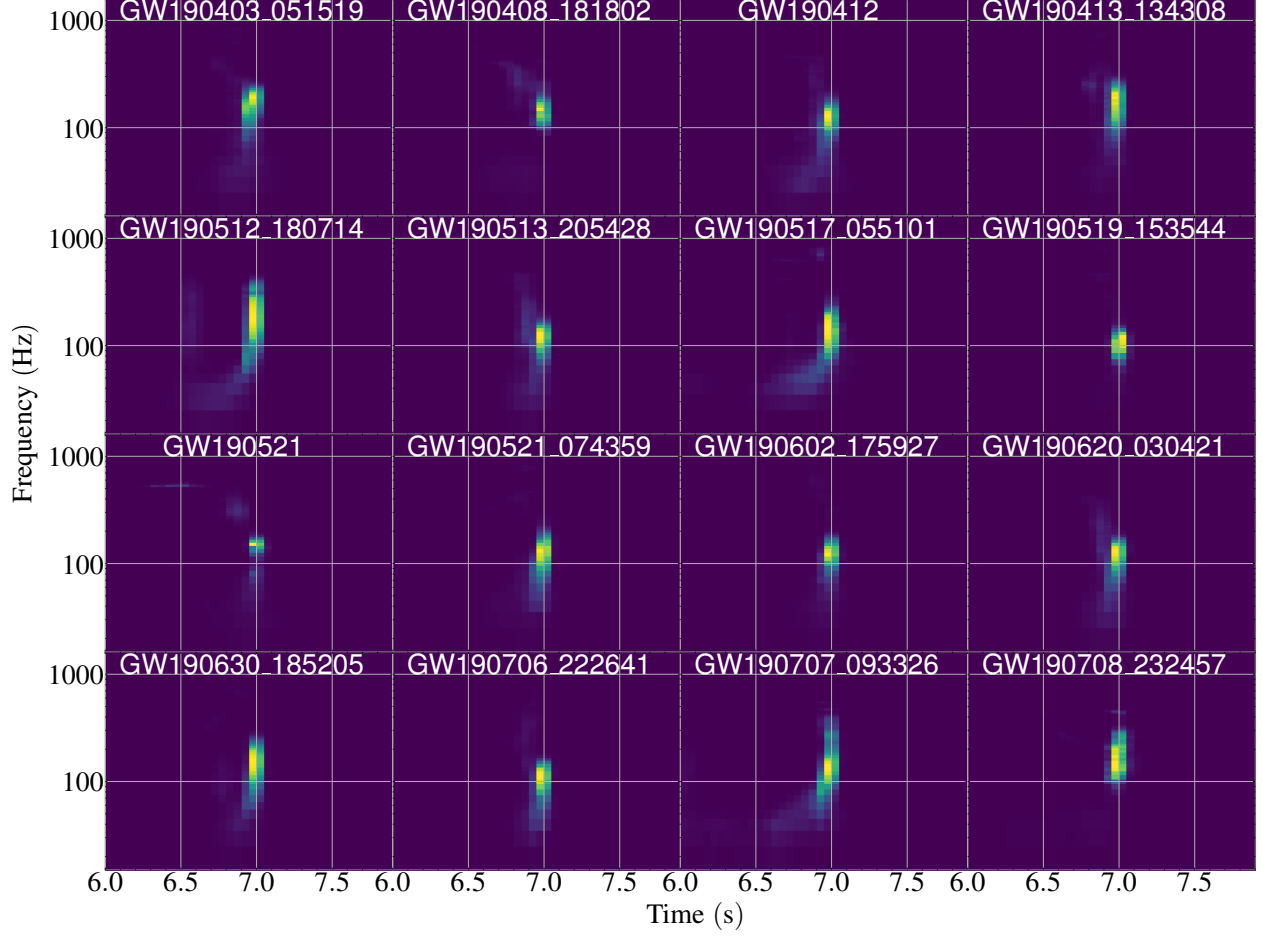


FIG. 8: The time-frequency representation of GW signals of O3 identified by the trained network are partially presented, with the remaining O3 signals presented in Appendix A. Note that in order to clearly show the identified results of O3, for each GW signal, we set the lower limit of the colorbar to 0, and the upper limit of the colorbar is determined by the maximum value of each event. For clarity, we only show the GW signals from 6 s to 8 s. For each GW signal, we only show the better-identified signal from LIGO Livingston or LIGO Hanford for simplicity.

Hanford and LIGO Livingston, i.e., we consider the signal identified as long as it is detected by either of the two detectors. Note that in the present work, we consider the identification of the GW signals from BBH mergers, so GW events involving NSs are not considered in this work (summarized in Table III).

In Fig. 7, we show the time-frequency representation of GW signals of O1 and O2 identified by the trained network. We can see that all the GW events are identified by the network. In fact, we also test the network by identifying BNS mergers and find that the

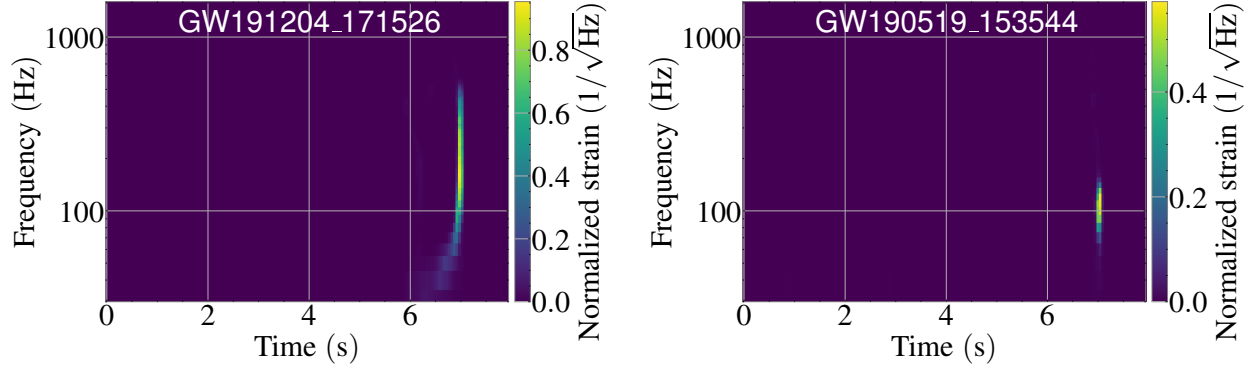


FIG. 9: The time-frequency representation of GW signals of the GW191204_171526 (chirp mass $\mathcal{M}_{\text{chirp}} = 19.21 M_{\odot}$) and GW190519_153544 (chirp mass $\mathcal{M}_{\text{chirp}} = 100 M_{\odot}$) identified by the network.

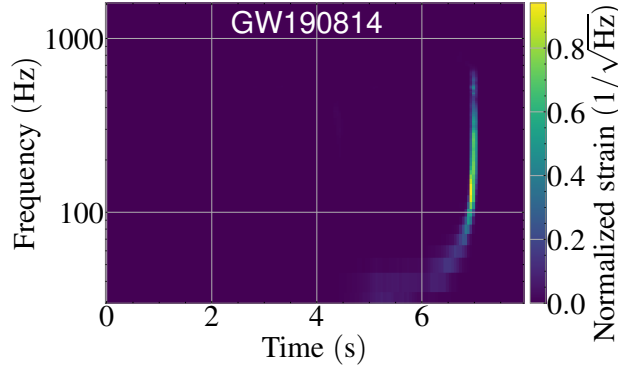


FIG. 10: The time-frequency representation of GW signal of the GW190814 identified by the network.

network is unable to identify them, which is consistent with our expectations. From the figure, we can also see that the identified signals obtained from the network are also different for different GW events. The prime cause is that the time-frequency signals of GW for different chirp masses are different. This also means that the time-frequency representation of GW signals identified by U-Net may be used to preliminarily determine the chirp masses of the GW sources. Previous work shows that the prior selection of the GW parameter has an important impact on the Bayesian inference [140]. Our results show that the network can not only rapidly and accurately identify the GW signals, but also provide great help for the later Bayesian inferences.

Subsequently, we apply the trained network to the identification of the O3 data. In Fig. 8,

we show the time-frequency representation of GW signals of O3 identified by the trained network. We can see that the trained network shows a strong ability to identify GW signals. The identified ability of O3 is better than that of O2 because we use the background noise of O3 to train. 58 GW signals are clearly identified through the network. Note that for O3, we consider a total of 73 GW signals for analysis and only show the identified results. About 80% (79.3%) GW signals of O3 could be rapidly and accurately identified. In Fig. 9, we show the time-frequency GW signals of the GW191204_171526 (chirp mass $\mathcal{M}_{\text{chirp}} = 19.21 M_{\odot}$) and GW190519_153544 (chirp mass $\mathcal{M}_{\text{chirp}} = 100 M_{\odot}$) identified by the trained network. We could see that the lower-mass GW signals have a longer duration in the time-frequency representation, so they exhibit a shape similar to a “tail”. While the higher-mass GW signals have a shorter duration and therefore appear as a sharp peak. It also means that the trained network shows the potential of providing mass priors. But when the network cuts out noise, it also cuts out part of the signal. Signals without a small tail may still have a small chirp mass. Here we want to emphasize that if we could see a long tail almost to the far left of the picture like GW190728_064510 (chirp mass $\mathcal{M}_{\text{chirp}} = 8.6 M_{\odot}$) and GW191103_012549 (chirp mass $\mathcal{M}_{\text{chirp}} = 8.34 M_{\odot}$) in Fig. 11, and GW191204_171526 (chirp mass $\mathcal{M}_{\text{chirp}} = 8.55 M_{\odot}$) and GW191216_213338 (chirp mass $\mathcal{M}_{\text{chirp}} = 8.33 M_{\odot}$) in Fig. 12, a prior judgment can be made that the chirp mass of this kind of signal is below $10 M_{\odot}$. If we could see a tail but not long like GW190412 (chirp mass $\mathcal{M}_{\text{chirp}} = 13.3 M_{\odot}$) in Fig. 11, another prior judgment can be made that the chirp mass of this kind of signal is below $35 M_{\odot}$.

Our results show the potential of the U-Net algorithm in identifying time-frequency GW signals and providing mass priors in the future. In addition, we also use the trained network to identify BNS mergers, NSBH mergers, and some uncertain events. We find that our network can not identify BNS and NSBH mergers, which is also in line with our expectations. However, GW190814 (the lightest BH or the heaviest NS) [141] is a special event that is successfully identified by our network, as shown in Fig. 10.

IV. CONCLUSION

In this work, we use the U-Net algorithm to identify time-frequency GW signals of LIGO O1, O2, and O3 observations. We trained the network using the dataset of pure background noise signals and the dataset of GW signal and background noise signal. In the test dataset,

the false alarm probabilities for O1, O2, and O3 are all better than 0.1%. The trained network is then used to identify the real observations. The time-frequency representation of GW signals of O1 and O2 are all identified. Moreover, due to the fact that the time-frequency representation of GW signals for different chirp masses are different, the identified time-frequency representation of GW signals by U-Net can be used to preliminarily determine the chirp masses of the GW sources. For O3, the trained network could identify about 80% GW events. Our results show that the U-Net algorithm could rapidly identify the time-frequency representation of GW signals from BBH mergers and provide rapid prior information for the Bayesian inferences. In addition, GW190814 is a special event that can also be identified by the network (other BNS mergers and NSBH mergers cannot be identified).

Acknowledgments

This research has made use of data or softwares obtained from the Gravitational Wave Open Science Center (gwosc.org), a service of LIGO Laboratory, the LIGO Scientific Collaboration, the Virgo Collaboration, and KAGRA. We thank He Wang for helpful discussions. This work was supported by the National SKA Program of China (Grants Nos. 2022SKA0110200 and 2022SKA0110203) and the National Natural Science Foundation of China (Grants Nos. 11975072, 11875102, and 11835009).

-
- [1] **LIGO Scientific, Virgo** Collaboration, B. P. Abbott et al., *Observation of Gravitational Waves from a Binary Black Hole Merger*, Phys. Rev. Lett. **116** (2016), no. 6 061102, [[arXiv:1602.03837](#)].
 - [2] A. Einstein, *Näherungsweise integration der feldgleichungen der gravitation*, Sitzungsberichte der Königlich Preußischen Akademie der Wissenschaften (1916) 688–696.
 - [3] **LIGO Scientific, Virgo** Collaboration, B. P. Abbott et al., *GW170817: Observation of Gravitational Waves from a Binary Neutron Star Inspiral*, Phys. Rev. Lett. **119** (2017), no. 16 161101, [[arXiv:1710.05832](#)].
 - [4] **LIGO Scientific, Virgo, Fermi GBM, INTEGRAL, IceCube, AstroSat**

- Cadmium Zinc Telluride Imager Team, IPN, Insight-Hxmt, ANTARES, Swift, AGILE Team, 1M2H Team, Dark Energy Camera GW-EM, DES, DLT40, GRAWITA, Fermi-LAT, ATCA, ASKAP, Las Cumbres Observatory Group, OzGrav, DWF (Deeper Wider Faster Program), AST3, CAASTRO, VINROUGE, MASTER, J-GEM, GROWTH, JAGWAR, CaltechNRAO, TTU-NRAO, NuSTAR, Pan-STARRS, MAXI Team, TZAC Consortium, KU, Nordic Optical Telescope, ePESSTO, GROND, Texas Tech University, SALT Group, TOROS, BOOTES, MWA, CALET, IKI-GW Follow-up, H.E.S.S., LOFAR, LWA, HAWC, Pierre Auger, ALMA, Euro VLBI Team, Pi of Sky, Chandra Team at McGill University, DFN, ATLAS Telescopes, High Time Resolution Universe Survey, RIMAS, RATIR, SKA South Africa/MeerKAT Collaboration, B. P. Abbott et al., *Multi-messenger Observations of a Binary Neutron Star Merger*, Astrophys. J. Lett. **848** (2017), no. 2 L12, [[arXiv:1710.05833](https://arxiv.org/abs/1710.05833)].
- [5] **LIGO Scientific** Collaboration, J. Aasi et al., *Advanced LIGO*, Class. Quant. Grav. **32** (2015) 074001, [[arXiv:1411.4547](https://arxiv.org/abs/1411.4547)].
- [6] **VIRGO** Collaboration, F. Acernese et al., *Advanced Virgo: a second-generation interferometric gravitational wave detector*, Class. Quant. Grav. **32** (2015), no. 2 024001, [[arXiv:1408.3978](https://arxiv.org/abs/1408.3978)].
- [7] **KAGRA** Collaboration, T. Akutsu et al., *KAGRA: 2.5 Generation Interferometric Gravitational Wave Detector*, Nature Astron. **3** (2019), no. 1 35–40, [[arXiv:1811.08079](https://arxiv.org/abs/1811.08079)].
- [8] <https://gwosc.org/eventapi/html/allevvents/>.
- [9] **LIGO Scientific, Virgo** Collaboration, B. P. Abbott et al., *GWTC-1: A Gravitational-Wave Transient Catalog of Compact Binary Mergers Observed by LIGO and Virgo during the First and Second Observing Runs*, Phys. Rev. X **9** (2019), no. 3 031040, [[arXiv:1811.12907](https://arxiv.org/abs/1811.12907)].
- [10] **LIGO Scientific, Virgo** Collaboration, R. Abbott et al., *GWTC-2: Compact Binary Coalescences Observed by LIGO and Virgo During the First Half of the Third Observing Run*, Phys. Rev. X **11** (2021) 021053, [[arXiv:2010.14527](https://arxiv.org/abs/2010.14527)].
- [11] **KAGRA, VIRGO, LIGO Scientific** Collaboration, R. Abbott et al., *GWTC-3: Compact Binary Coalescences Observed by LIGO and Virgo during the Second Part of the Third Observing Run*, Phys. Rev. X **13** (2023), no. 4 041039, [[arXiv:2111.03606](https://arxiv.org/abs/2111.03606)].

- [12] **LIGO Scientific, VIRGO** Collaboration, R. Abbott et al., *GWTC-2.1: Deep extended catalog of compact binary coalescences observed by LIGO and Virgo during the first half of the third observing run*, Phys. Rev. D **109** (2024), no. 2 022001, [[arXiv:2108.01045](#)].
- [13] E. Berti et al., *Testing General Relativity with Present and Future Astrophysical Observations*, Class. Quant. Grav. **32** (2015) 243001, [[arXiv:1501.07274](#)].
- [14] **LIGO Scientific, Virgo** Collaboration, B. P. Abbott et al., *Tests of general relativity with GW150914*, Phys. Rev. Lett. **116** (2016), no. 22 221101, [[arXiv:1602.03841](#)]. [Erratum: Phys.Rev.Lett. 121, 129902 (2018)].
- [15] **LIGO Scientific, Virgo** Collaboration, B. P. Abbott et al., *Tests of General Relativity with GW170817*, Phys. Rev. Lett. **123** (2019), no. 1 011102, [[arXiv:1811.00364](#)].
- [16] **LIGO Scientific, Virgo** Collaboration, B. P. Abbott et al., *Tests of General Relativity with the Binary Black Hole Signals from the LIGO-Virgo Catalog GWTC-1*, Phys. Rev. D **100** (2019), no. 10 104036, [[arXiv:1903.04467](#)].
- [17] **LIGO Scientific, Virgo** Collaboration, R. Abbott et al., *Tests of general relativity with binary black holes from the second LIGO-Virgo gravitational-wave transient catalog*, Phys. Rev. D **103** (2021), no. 12 122002, [[arXiv:2010.14529](#)].
- [18] **LIGO Scientific, VIRGO, KAGRA** Collaboration, R. Abbott et al., *Tests of General Relativity with GWTC-3*, [arXiv:2112.06861](#).
- [19] C. Gong, T. Zhu, R. Niu, Q. Wu, J.-L. Cui, X. Zhang, W. Zhao, and A. Wang, *Gravitational wave constraints on Lorentz and parity violations in gravity: High-order spatial derivative cases*, Phys. Rev. D **105** (2022), no. 4 044034, [[arXiv:2112.06446](#)].
- [20] C. Gong, T. Zhu, R. Niu, Q. Wu, J.-L. Cui, X. Zhang, W. Zhao, and A. Wang, *Gravitational wave constraints on nonbirefringent dispersions of gravitational waves due to Lorentz violations with GWTC-3 events*, Phys. Rev. D **107** (2023), no. 12 124015, [[arXiv:2302.05077](#)].
- [21] I. Mandel and F. S. Broekgaarden, *Rates of compact object coalescences*, Living Rev. Rel. **25** (2022), no. 1 1, [[arXiv:2107.14239](#)].
- [22] L. A. C. van Son, S. E. de Mink, T. Callister, S. Justham, M. Renzo, T. Wagg, F. S. Broekgaarden, F. Kummer, R. Pakmor, and I. Mandel, *The Redshift Evolution of the Binary Black Hole Merger Rate: A Weighty Matter*, Astrophys. J. **931** (2022), no. 1 17, [[arXiv:2110.01634](#)].

- [23] F. S. Broekgaarden et al., *Impact of Massive Binary Star and Cosmic Evolution on Gravitational Wave Observations II: Double Compact Object Rates and Properties*, [arXiv:2112.05763](#).
- [24] J. M. Ezquiaga and D. E. Holz, *Spectral Sirens: Cosmology from the Full Mass Distribution of Compact Binaries*, Phys. Rev. Lett. **129** (2022), no. 6 061102, [[arXiv:2202.08240](#)].
- [25] **LIGO Scientific, Virgo, 1M2H, Dark Energy Camera GW-E, DES, DLT40, Las Cumbres Observatory, VINROUGE, MASTER** Collaboration, B. P. Abbott et al., *A gravitational-wave standard siren measurement of the Hubble constant*, Nature **551** (2017), no. 7678 85–88, [[arXiv:1710.05835](#)].
- [26] H.-Y. Chen, M. Fishbach, and D. E. Holz, *A two per cent Hubble constant measurement from standard sirens within five years*, Nature **562** (2018), no. 7728 545–547, [[arXiv:1712.06531](#)].
- [27] **LIGO Scientific, Virgo, KAGRA** Collaboration, R. Abbott et al., *Constraints on the Cosmic Expansion History from GWTC–3*, Astrophys. J. **949** (2023), no. 2 76, [[arXiv:2111.03604](#)].
- [28] **DES, LIGO Scientific, Virgo** Collaboration, M. Soares-Santos et al., *First Measurement of the Hubble Constant from a Dark Standard Siren using the Dark Energy Survey Galaxies and the LIGO/Virgo Binary–Black-hole Merger GW170814*, Astrophys. J. Lett. **876** (2019), no. 1 L7, [[arXiv:1901.01540](#)].
- [29] **DES** Collaboration, A. Palmese et al., *A statistical standard siren measurement of the Hubble constant from the LIGO/Virgo gravitational wave compact object merger GW190814 and Dark Energy Survey galaxies*, Astrophys. J. Lett. **900** (2020), no. 2 L33, [[arXiv:2006.14961](#)].
- [30] **LIGO Scientific, Virgo, VIRGO** Collaboration, B. P. Abbott et al., *A Gravitational-wave Measurement of the Hubble Constant Following the Second Observing Run of Advanced LIGO and Virgo*, Astrophys. J. **909** (2021), no. 2 218, [[arXiv:1908.06060](#)].
- [31] D. E. Holz and S. A. Hughes, *Using gravitational-wave standard sirens*, Astrophys. J. **629** (2005) 15–22, [[astro-ph/0504616](#)].
- [32] N. Dalal, D. E. Holz, S. A. Hughes, and B. Jain, *Short grb and binary black hole standard sirens as a probe of dark energy*, Phys. Rev. D **74** (2006) 063006, [[astro-ph/0601275](#)].

- [33] S. Nissanke, D. E. Holz, S. A. Hughes, N. Dalal, and J. L. Sievers, *Exploring short gamma-ray bursts as gravitational-wave standard sirens*, Astrophys. J. **725** (2010) 496–514, [[arXiv:0904.1017](#)].
- [34] C. Cutler and D. E. Holz, *Ultra-high precision cosmology from gravitational waves*, Phys. Rev. D **80** (2009) 104009, [[arXiv:0906.3752](#)].
- [35] S. Camera and A. Nishizawa, *Beyond Concordance Cosmology with Magnification of Gravitational-Wave Standard Sirens*, Phys. Rev. Lett. **110** (2013), no. 15 151103, [[arXiv:1303.5446](#)].
- [36] S. Vitale and H.-Y. Chen, *Measuring the Hubble constant with neutron star black hole mergers*, Phys. Rev. Lett. **121** (2018), no. 2 021303, [[arXiv:1804.07337](#)].
- [37] L. Bian et al., *The Gravitational-wave physics II: Progress*, Sci. China Phys. Mech. Astron. **64** (2021), no. 12 120401, [[arXiv:2106.10235](#)].
- [38] R.-G. Cai and T. Yang, *Estimating cosmological parameters by the simulated data of gravitational waves from the Einstein Telescope*, Phys. Rev. D **95** (2017), no. 4 044024, [[arXiv:1608.08008](#)].
- [39] R.-G. Cai, T.-B. Liu, X.-W. Liu, S.-J. Wang, and T. Yang, *Probing cosmic anisotropy with gravitational waves as standard sirens*, Phys. Rev. D **97** (2018), no. 10 103005, [[arXiv:1712.00952](#)].
- [40] R.-G. Cai and T. Yang, *Standard sirens and dark sector with Gaussian process*, EPJ Web Conf. **168** (2018) 01008, [[arXiv:1709.00837](#)].
- [41] X. Zhang, *Gravitational wave standard sirens and cosmological parameter measurement*, Sci. China Phys. Mech. Astron. **62** (2019), no. 11 110431, [[arXiv:1905.11122](#)].
- [42] H.-Y. Chen, *Systematic Uncertainty of Standard Sirens from the Viewing Angle of Binary Neutron Star Inspirals*, Phys. Rev. Lett. **125** (2020), no. 20 201301, [[arXiv:2006.02779](#)].
- [43] R. Gray et al., *Cosmological inference using gravitational wave standard sirens: A mock data analysis*, Phys. Rev. D **101** (2020), no. 12 122001, [[arXiv:1908.06050](#)].
- [44] W. Zhao, C. Van Den Broeck, D. Baskaran, and T. G. F. Li, *Determination of Dark Energy by the Einstein Telescope: Comparing with CMB, BAO and SNIa Observations*, Phys. Rev. D **83** (2011) 023005, [[arXiv:1009.0206](#)].
- [45] W. Zhao, B. S. Wright, and B. Li, *Constraining the time variation of Newton’s constant G with gravitational-wave standard sirens and supernovae*, JCAP **10** (2018) 052,

- [[arXiv:1804.03066](#)].
- [46] S.-J. Jin, T.-N. Li, J.-F. Zhang, and X. Zhang, *Prospects for measuring the Hubble constant and dark energy using gravitational-wave dark sirens with neutron star tidal deformation*, JCAP **08** (2023) 070, [[arXiv:2202.11882](#)].
- [47] M. Du, W. Yang, L. Xu, S. Pan, and D. F. Mota, *Future constraints on dynamical dark-energy using gravitational-wave standard sirens*, Phys. Rev. D **100** (2019), no. 4 043535, [[arXiv:1812.01440](#)].
- [48] Y.-F. Cai, C. Li, E. N. Saridakis, and L. Xue, *$f(T)$ gravity after GW170817 and GRB170817A*, Phys. Rev. D **97** (2018), no. 10 103513, [[arXiv:1801.05827](#)].
- [49] W. Yang, S. Pan, E. Di Valentino, B. Wang, and A. Wang, *Forecasting interacting vacuum-energy models using gravitational waves*, JCAP **05** (2020) 050, [[arXiv:1904.11980](#)].
- [50] W. Yang, S. Vagnozzi, E. Di Valentino, R. C. Nunes, S. Pan, and D. F. Mota, *Listening to the sound of dark sector interactions with gravitational wave standard sirens*, JCAP **07** (2019) 037, [[arXiv:1905.08286](#)].
- [51] R. R. A. Bachega, A. A. Costa, E. Abdalla, and K. S. F. Fornazier, *Forecasting the Interaction in Dark Matter-Dark Energy Models with Standard Sirens From the Einstein Telescope*, JCAP **05** (2020) 021, [[arXiv:1906.08909](#)].
- [52] Z. Chang, Q.-G. Huang, S. Wang, and Z.-C. Zhao, *Low-redshift constraints on the Hubble constant from the baryon acoustic oscillation “standard rulers” and the gravitational wave “standard sirens”*, Eur. Phys. J. C **79** (2019), no. 2 177.
- [53] J.-F. Zhang, M. Zhang, S.-J. Jin, J.-Z. Qi, and X. Zhang, *Cosmological parameter estimation with future gravitational wave standard siren observation from the Einstein Telescope*, JCAP **09** (2019) 068, [[arXiv:1907.03238](#)].
- [54] S. Mukherjee, G. Lavaux, F. R. Bouchet, J. Jasche, B. D. Wandelt, S. M. Nissanke, F. Leclercq, and K. Hotokezaka, *Velocity correction for Hubble constant measurements from standard sirens*, Astron. Astrophys. **646** (2021) A65, [[arXiv:1909.08627](#)].
- [55] J.-h. He, *Accurate method to determine the systematics due to the peculiar velocities of galaxies in measuring the Hubble constant from gravitational-wave standard sirens*, Phys. Rev. D **100** (2019), no. 2 023527, [[arXiv:1903.11254](#)].
- [56] Z.-W. Zhao, L.-F. Wang, J.-F. Zhang, and X. Zhang, *Prospects for improving cosmological*

- parameter estimation with gravitational-wave standard sirens from Taiji*, Sci. Bull. **65** (2020), no. 16 1340–1348, [[arXiv:1912.11629](#)].
- [57] L.-F. Wang, S.-J. Jin, J.-F. Zhang, and X. Zhang, *Forecast for cosmological parameter estimation with gravitational-wave standard sirens from the LISA-Taiji network*, Sci. China Phys. Mech. Astron. **65** (2022), no. 1 210411, [[arXiv:2101.11882](#)].
- [58] J.-Z. Qi, S.-J. Jin, X.-L. Fan, J.-F. Zhang, and X. Zhang, *Using a multi-messenger and multi-wavelength observational strategy to probe the nature of dark energy through direct measurements of cosmic expansion history*, JCAP **12** (2021), no. 12 042, [[arXiv:2102.01292](#)].
- [59] S.-J. Jin, L.-F. Wang, P.-J. Wu, J.-F. Zhang, and X. Zhang, *How can gravitational-wave standard sirens and 21-cm intensity mapping jointly provide a precise late-universe cosmological probe?*, Phys. Rev. D **104** (2021), no. 10 103507, [[arXiv:2106.01859](#)].
- [60] L.-G. Zhu, L.-H. Xie, Y.-M. Hu, S. Liu, E.-K. Li, N. R. Napolitano, B.-T. Tang, J.-d. Zhang, and J. Mei, *Constraining the Hubble constant to a precision of about 1% using multi-band dark standard siren detections*, Sci. China Phys. Mech. Astron. **65** (2022), no. 5 259811, [[arXiv:2110.05224](#)].
- [61] J. M. S. de Souza, R. Sturani, and J. Alcaniz, *Cosmography with standard sirens from the Einstein Telescope*, JCAP **03** (2022), no. 03 025, [[arXiv:2110.13316](#)].
- [62] S.-J. Jin, R.-Q. Zhu, L.-F. Wang, H.-L. Li, J.-F. Zhang, and X. Zhang, *Impacts of gravitational-wave standard siren observations from Einstein Telescope and Cosmic Explorer on weighing neutrinos in interacting dark energy models*, Commun. Theor. Phys. **74** (2022), no. 10 105404, [[arXiv:2204.04689](#)].
- [63] M.-D. Cao, J. Zheng, J.-Z. Qi, X. Zhang, and Z.-H. Zhu, *A New Way to Explore Cosmological Tensions Using Gravitational Waves and Strong Gravitational Lensing*, Astrophys. J. **934** (2022), no. 2 108, [[arXiv:2112.14564](#)].
- [64] H. Leandro, V. Marra, and R. Sturani, *Measuring the Hubble constant with black sirens*, Phys. Rev. D **105** (2022), no. 2 023523, [[arXiv:2109.07537](#)].
- [65] X. Fu, L. Zhou, J. Yang, Z.-Y. Lu, Y. Yang, and G. Tang, *Exploring the potentiality of future standard candles and standard sirens to detect cosmic opacity*, Chin. Phys. C **45** (2021), no. 6 065104.
- [66] C. Ye and M. Fishbach, *Cosmology with standard sirens at cosmic noon*, Phys. Rev. D **104**

- (2021), no. 4 043507, [[arXiv:2103.14038](#)].
- [67] H.-Y. Chen, P. S. Cowperthwaite, B. D. Metzger, and E. Berger, *A Program for Multimessenger Standard Siren Cosmology in the Era of LIGO A+, Rubin Observatory, and Beyond*, Astrophys. J. Lett. **908** (2021), no. 1 L4, [[arXiv:2011.01211](#)].
- [68] A. Mitra, J. Mifsud, D. F. Mota, and D. Parkinson, *Cosmology with the Einstein Telescope: No Slip Gravity Model and Redshift Specifications*, Mon. Not. Roy. Astron. Soc. **502** (2021), no. 4 5563–5575, [[arXiv:2010.00189](#)].
- [69] N. B. Hogg, M. Martinelli, and S. Nesseris, *Constraints on the distance duality relation with standard sirens*, JCAP **12** (2020) 019, [[arXiv:2007.14335](#)].
- [70] R. C. Nunes, *Searching for modified gravity in the astrophysical gravitational wave background: Application to ground-based interferometers*, Phys. Rev. D **102** (2020), no. 2 024071, [[arXiv:2007.07750](#)].
- [71] S. Borhanian, A. Dhani, A. Gupta, K. G. Arun, and B. S. Sathyaprakash, *Dark Sirens to Resolve the Hubble–Lemaître Tension*, Astrophys. J. Lett. **905** (2020), no. 2 L28, [[arXiv:2007.02883](#)].
- [72] S.-J. Jin, D.-Z. He, Y. Xu, J.-F. Zhang, and X. Zhang, *Forecast for cosmological parameter estimation with gravitational-wave standard siren observation from the Cosmic Explorer*, JCAP **03** (2020) 051, [[arXiv:2001.05393](#)].
- [73] J. Yu, Y. Wang, W. Zhao, and Y. Lu, *Hunting for the host galaxy groups of binary black holes and the application in constraining Hubble constant*, Mon. Not. Roy. Astron. Soc. **498** (2020), no. 2 1786–1800, [[arXiv:2003.06586](#)].
- [74] S.-J. Jin, S.-S. Xing, Y. Shao, J.-F. Zhang, and X. Zhang, *Joint constraints on cosmological parameters using future multi-band gravitational wave standard siren observations*, Chin. Phys. C **47** (2023) 065104, [[arXiv:2301.06722](#)].
- [75] S.-J. Jin, Y.-Z. Zhang, J.-Y. Song, J.-F. Zhang, and X. Zhang, *Taiji-TianQin-LISA network: Precisely measuring the Hubble constant using both bright and dark sirens*, Sci. China Phys. Mech. Astron. **67** (2024), no. 2 220412, [[arXiv:2305.19714](#)].
- [76] S.-J. Jin, R.-Q. Zhu, J.-Y. Song, T. Han, J.-F. Zhang, and X. Zhang, *Standard siren cosmology in the era of the 2.5-generation ground-based gravitational wave detectors: bright and dark sirens of LIGO Voyager and NEMO*, [arXiv:2309.11900](#).
- [77] T. Han, S.-J. Jin, J.-F. Zhang, and X. Zhang, *A comprehensive forecast for cosmological*

- parameter estimation using joint observations of gravitational-wave standard sirens and short γ -ray bursts*, [arXiv:2309.14965](#).
- [78] T.-N. Li, S.-J. Jin, H.-L. Li, J.-F. Zhang, and X. Zhang, *Prospects for Probing the Interaction between Dark Energy and Dark Matter Using Gravitational-wave Dark Sirens with Neutron Star Tidal Deformation*, Astrophys. J. **963** (2024), no. 1 52, [[arXiv:2310.15879](#)].
 - [79] **LIGO Scientific, Virgo** Collaboration, B. P. Abbott et al., *Search for intermediate mass black hole binaries in the first and second observing runs of the Advanced LIGO and Virgo network*, Phys. Rev. D **100** (2019), no. 6 064064, [[arXiv:1906.08000](#)].
 - [80] R. Magee et al., *First demonstration of early warning gravitational wave alerts*, Astrophys. J. Lett. **910** (2021), no. 2 L21, [[arXiv:2102.04555](#)].
 - [81] H. Xia, L. Shao, J. Zhao, and Z. Cao, *Improved deep learning techniques in gravitational-wave data analysis*, Phys. Rev. D **103** (2021), no. 2 024040, [[arXiv:2011.04418](#)].
 - [82] Y. LeCun, Y. Bengio, and G. Hinton, *Deep learning*, nature **521** (2015), no. 7553 436–444.
 - [83] D. Guest, K. Cranmer, and D. Whiteson, *Deep learning and its application to lhc physics*, Annual Review of Nuclear and Particle Science **68** (2018) 161–181.
 - [84] P. Baldi, P. Sadowski, and D. Whiteson, *Searching for Exotic Particles in High-Energy Physics with Deep Learning*, Nature Commun. **5** (2014) 4308, [[arXiv:1402.4735](#)].
 - [85] D. Guest, K. Cranmer, and D. Whiteson, *Deep Learning and its Application to LHC Physics*, Ann. Rev. Nucl. Part. Sci. **68** (2018) 161–181, [[arXiv:1806.11484](#)].
 - [86] W. Wei and E. A. Huerta, *Gravitational Wave Denoising of Binary Black Hole Mergers with Deep Learning*, Phys. Lett. B **800** (2020) 135081, [[arXiv:1901.00869](#)].
 - [87] D. George, H. Shen, and E. A. Huerta, *Deep Transfer Learning: A new deep learning glitch classification method for advanced LIGO*, [arXiv:1706.07446](#).
 - [88] C. Chatterjee, L. Wen, K. Vinsen, M. Kovalam, and A. Datta, *Using Deep Learning to Localize Gravitational Wave Sources*, Phys. Rev. D **100** (2019), no. 10 103025, [[arXiv:1909.06367](#)].
 - [89] H. Shen, D. George, E. A. Huerta, and Z. Zhao, *Denoising Gravitational Waves with Enhanced Deep Recurrent Denoising Auto-Encoders*, [arXiv:1903.03105](#).
 - [90] E. Cuoco et al., *Enhancing Gravitational-Wave Science with Machine Learning*, Mach.

- Learn. Sci. Tech. **2** (2021), no. 1 011002, [[arXiv:2005.03745](#)].
- [91] J. a. D. Álvares, J. A. Font, F. F. Freitas, O. G. Freitas, A. P. Morais, S. Nunes, A. Onofre, and A. Torres-Forné, *Gravitational-wave parameter inference using Deep Learning*, 11, 2020. [arXiv:2011.10425](#).
 - [92] S. R. Green, C. Simpson, and J. Gair, *Gravitational-wave parameter estimation with autoregressive neural network flows*, Phys. Rev. D **102** (2020), no. 10 104057, [[arXiv:2002.07656](#)].
 - [93] S. R. Green and J. Gair, *Complete parameter inference for GW150914 using deep learning*, Mach. Learn. Sci. Tech. **2** (2021), no. 3 03LT01, [[arXiv:2008.03312](#)].
 - [94] M. Dax, S. R. Green, J. Gair, M. Pürrer, J. Wildberger, J. H. Macke, A. Buonanno, and B. Schölkopf, *Neural Importance Sampling for Rapid and Reliable Gravitational-Wave Inference*, Phys. Rev. Lett. **130** (2023), no. 17 171403, [[arXiv:2210.05686](#)].
 - [95] J. P. Marulanda, C. Santa, and A. E. Romano, *Deep learning merger masses estimation from gravitational waves signals in the frequency domain*, Phys. Lett. B **810** (2020) 135790, [[arXiv:2004.01050](#)].
 - [96] S. Singh, A. Singh, A. Prajapati, and K. N. Pathak, *Deep learning for estimating parameters of gravitational waves*, Mon. Not. Roy. Astron. Soc. **508** (2021), no. 1 1358–1370, [[arXiv:2008.06550](#)].
 - [97] M. Mould, D. Gerosa, and S. R. Taylor, *Deep learning and Bayesian inference of gravitational-wave populations: Hierarchical black-hole mergers*, Phys. Rev. D **106** (2022), no. 10 103013, [[arXiv:2203.03651](#)].
 - [98] C. Chatterjee, L. Wen, F. Diakogiannis, and K. Vinsen, *Extraction of binary black hole gravitational wave signals from detector data using deep learning*, Phys. Rev. D **104** (2021), no. 6 064046, [[arXiv:2105.03073](#)].
 - [99] A. McLeod, D. Jacobs, C. Chatterjee, L. Wen, and F. Panther, *Rapid Mass Parameter Estimation of Binary Black Hole Coalescences Using Deep Learning*, [arXiv:2201.11126](#).
 - [100] J. Langendorff, A. Kolmus, J. Janquart, and C. Van Den Broeck, *Normalizing Flows as an Avenue to Studying Overlapping Gravitational Wave Signals*, Phys. Rev. Lett. **130** (2023), no. 17 171402, [[arXiv:2211.15097](#)].
 - [101] C. Chatterjee, M. Kovalam, L. Wen, D. Beveridge, F. Diakogiannis, and K. Vinsen, *Rapid Localization of Gravitational Wave Sources from Compact Binary Coalescences Using Deep*

- Learning*, Astrophys. J. **959** (2023), no. 1 42, [[arXiv:2207.14522](#)].
- [102] T.-Y. Sun, C.-Y. Xiong, S.-J. Jin, Y.-X. Wang, J.-F. Zhang, and X. Zhang, *Efficient parameter inference for gravitational wave signals in the presence of transient noises using temporal and time-spectral fusion normalizing flow*, [arXiv:2312.08122](#).
- [103] D. George and E. A. Huerta, *Deep Neural Networks to Enable Real-time Multimessenger Astrophysics*, Phys. Rev. D **97** (2018), no. 4 044039, [[arXiv:1701.00008](#)].
- [104] H. Gabbard, M. Williams, F. Hayes, and C. Messenger, *Matching matched filtering with deep networks for gravitational-wave astronomy*, Phys. Rev. Lett. **120** (2018), no. 14 141103, [[arXiv:1712.06041](#)].
- [105] P. G. Krastev, K. Gill, V. A. Villar, and E. Berger, *Detection and Parameter Estimation of Gravitational Waves from Binary Neutron-Star Mergers in Real LIGO Data using Deep Learning*, Phys. Lett. B **815** (2021) 136161, [[arXiv:2012.13101](#)].
- [106] M. Cabero, A. Mahabal, and J. McIver, *GWSkyNet: a real-time classifier for public gravitational-wave candidates*, Astrophys. J. Lett. **904** (2020), no. 1 L9, [[arXiv:2010.11829](#)].
- [107] S. Jadhav, N. Mukund, B. Gadre, S. Mitra, and S. Abraham, *Improving significance of binary black hole mergers in Advanced LIGO data using deep learning: Confirmation of GW151216*, Phys. Rev. D **104** (2021), no. 6 064051, [[arXiv:2010.08584](#)].
- [108] D. George and E. A. Huerta, *Deep Learning for Real-time Gravitational Wave Detection and Parameter Estimation: Results with Advanced LIGO Data*, Phys. Lett. B **778** (2018) 64–70, [[arXiv:1711.03121](#)].
- [109] X. Fan, J. Li, X. Li, Y. Zhong, and J. Cao, *Applying deep neural networks to the detection and space parameter estimation of compact binary coalescence with a network of gravitational wave detectors*, Sci. China Phys. Mech. Astron. **62** (2019), no. 6 969512, [[arXiv:1811.01380](#)].
- [110] 1909.13442, S. Wu, Z. Cao, X. Liu, and J.-Y. Zhu, *Gravitational-wave signal recognition of LIGO data by deep learning*, Phys. Rev. D **101** (2020), no. 10 104003, [[arXiv:1909.13442](#)].
- [111] P. G. Krastev, *Real-Time Detection of Gravitational Waves from Binary Neutron Stars using Artificial Neural Networks*, Phys. Lett. B **803** (2020) 135330, [[arXiv:1908.03151](#)].
- [112] W. Wei, A. Khan, E. A. Huerta, X. Huang, and M. Tian, *Deep Learning Ensemble for Real-time Gravitational Wave Detection of Spinning Binary Black Hole Mergers*, Phys.

- Lett. B **812** (2021) 136029, [[arXiv:2010.15845](#)].
- [113] C. Verma, A. Reza, D. Krishnaswamy, S. Caudill, and G. Gaur, *Employing deep learning for detection of gravitational waves from compact binary coalescences*, AIP Conf. Proc. **2555** (2022), no. 1 020010, [[arXiv:2110.01883](#)].
 - [114] E. A. Moreno, B. Borzyszkowski, M. Pierini, J.-R. Vlimant, and M. Spiropulu, *Source-agnostic gravitational-wave detection with recurrent autoencoders*, Mach. Learn. Sci. Tech. **3** (2022), no. 2 025001, [[arXiv:2107.12698](#)].
 - [115] Y. Zhang, H. Xu, M. Liu, C. Liu, Y. Zhao, and J. Zhu, *Deep learning model based on a bidirectional gated recurrent unit for the detection of gravitational wave signals*, Phys. Rev. D **106** (2022), no. 12 122002.
 - [116] R. Qiu, P. G. Krastev, K. Gill, and E. Berger, *Deep learning detection and classification of gravitational waves from neutron star-black hole mergers*, Phys. Lett. B **840** (2023) 137850, [[arXiv:2210.15888](#)].
 - [117] P. Nousi, A. E. Koloniari, N. Passalis, P. Iosif, N. Stergioulas, and A. Tefas, *Deep residual networks for gravitational wave detection*, Phys. Rev. D **108** (2023), no. 2 024022, [[arXiv:2211.01520](#)].
 - [118] C. Ma, W. Wang, H. Wang, and Z. Cao, *Ensemble of deep convolutional neural networks for real-time gravitational wave signal recognition*, Phys. Rev. D **105** (2022), no. 8 083013, [[arXiv:2204.12058](#)].
 - [119] M. B. Schäfer et al., *First machine learning gravitational-wave search mock data challenge*, Phys. Rev. D **107** (2023), no. 2 023021, [[arXiv:2209.11146](#)].
 - [120] A. Trovato, E. Chassande-Mottin, M. Bejger, R. Flamary, and N. Courty, *Neural network time-series classifiers for gravitational-wave searches in single-detector periods*, [arXiv:2307.09268](#).
 - [121] M. B. Schäfer, O. Zelenka, A. H. Nitz, F. Ohme, and B. Brügmann, *Training strategies for deep learning gravitational-wave searches*, Phys. Rev. D **105** (2022), no. 4 043002, [[arXiv:2106.03741](#)].
 - [122] T. Marianer, D. Poznanski, and J. X. Prochaska, *A semisupervised machine learning search for never-seen gravitational-wave sources*, Mon. Not. Roy. Astron. Soc. **500** (2020), no. 4 5408–5419, [[arXiv:2010.11949](#)].
 - [123] V. Boudart and M. Fays, *Machine learning algorithm for minute-long burst searches*, Phys.

- Rev. D **105** (2022), no. 8 083007, [[arXiv:2201.08727](#)].
- [124] A. Ravichandran, A. Vijaykumar, S. J. Kapadia, and P. Kumar, *Rapid Identification and Classification of Eccentric Gravitational Wave Inspirals with Machine Learning*, [arXiv:2302.00666](#).
- [125] O. Ronneberger, P. Fischer, and T. Brox, *U-net: Convolutional networks for biomedical image segmentation*, in Medical Image Computing and Computer-Assisted Intervention–MICCAI 2015: 18th International Conference, Munich, Germany, October 5–9, 2015, Proceedings, Part III **18**, pp. 234–241, Springer, 2015.
- [126] S. Ni, Y. Li, L.-Y. Gao, and X. Zhang, *Eliminating Primary Beam Effect in Foreground Subtraction of Neutral Hydrogen Intensity Mapping Survey with Deep Learning*, Astrophys. J. **934** (2022), no. 1 83, [[arXiv:2204.02780](#)].
- [127] L.-Y. Gao, Y. Li, S. Ni, and X. Zhang, *Eliminating polarization leakage effect for neutral hydrogen intensity mapping with deep learning*, Mon. Not. Roy. Astron. Soc. **525** (2023), no. 4 5278–5290, [[arXiv:2212.08773](#)].
- [128] C. Devine, Z. B. Etienne, and S. T. McWilliams, *Optimizing spinning time-domain gravitational waveforms for Advanced LIGO data analysis*, Class. Quant. Grav. **33** (2016), no. 12 125025, [[arXiv:1601.03393](#)].
- [129] A. Bohé et al., *Improved effective-one-body model of spinning, nonprecessing binary black holes for the era of gravitational-wave astrophysics with advanced detectors*, Phys. Rev. D **95** (2017), no. 4 044028, [[arXiv:1611.03703](#)].
- [130] A. Nitz, I. Harry, D. Brown, C. M. Biwer, J. Willis, T. D. Canton, C. Capano, T. Dent, L. Pekowsky, S. De, M. Cabero, G. S. C. Davies, A. R. Williamson, D. Macleod, B. Machenschalk, F. Pannarale, P. Kumar, S. Reyes, dfinstad, S. Kumar, S. Wu, M. Tápai, L. Singer, veronica villa, S. Khan, S. Fairhurst, K. Chandra, A. Nielsen, S. Singh, and T. Massinger, *gwastro/pycbc: v2.1.2 release of pycbc*, May, 2023.
- [131] G. Baltus, J. Janquart, M. Lopez, H. Narola, and J.-R. Cudell, *Convolutional neural network for gravitational-wave early alert: Going down in frequency*, Phys. Rev. D **106** (2022), no. 4 042002, [[arXiv:2205.04750](#)].
- [132] <https://github.com/HarisIqbal88/PlotNeuralNet>.
- [133] D. M. Macleod, J. S. Areeda, S. B. Coughlin, T. J. Massinger, and A. L. Urban, *GWpy: A Python package for gravitational-wave astrophysics*, SoftwareX **13** (2021) 100657.

- [134] S. J. Reddi, S. Kale, and S. Kumar, *On the convergence of adam and beyond*, arXiv preprint arXiv:1904.09237 (2019).
- [135] T. Fawcett, *An introduction to roc analysis*, Pattern recognition letters **27** (2006), no. 8 861–874.
- [136] D. M. Powers, *Evaluation: from precision, recall and f-measure to roc, informedness, markedness and correlation*, arXiv preprint arXiv:2010.16061 (2020).
- [137] F. P. Barone, D. Dell’Aquila, and M. Russo, *A novel multi-layer modular approach for real-time fuzzy-identification of gravitational-wave signals*, Mach. Learn. Sci. Tech. **4** (2023), no. 4 045054, [[arXiv:2206.06004](#)].
- [138] M. Cabero et al., *Blip glitches in Advanced LIGO data*, Class. Quant. Grav. **36** (2019), no. 15 15, [[arXiv:1901.05093](#)].
- [139] A. H. Nitz, *Distinguishing short duration noise transients in LIGO data to improve the PyCBC search for gravitational waves from high mass binary black hole mergers*, Class. Quant. Grav. **35** (2018), no. 3 035016, [[arXiv:1709.08974](#)].
- [140] S. Vitale, D. Gerosa, C.-J. Haster, K. Chatziioannou, and A. Zimmerman, *Impact of Bayesian Priors on the Characterization of Binary Black Hole Coalescences*, Phys. Rev. Lett. **119** (2017), no. 25 251103, [[arXiv:1707.04637](#)].
- [141] **LIGO Scientific, Virgo Collaboration**, R. Abbott et al., *GW190814: Gravitational Waves from the Coalescence of a 23 Solar Mass Black Hole with a 2.6 Solar Mass Compact Object*, Astrophys. J. Lett. **896** (2020), no. 2 L44, [[arXiv:2006.12611](#)].

Appendix A: Results of U-Net

We present the remaining time-frequency GW events of O2 and O3 identified by the trained network in Appendix [A](#).

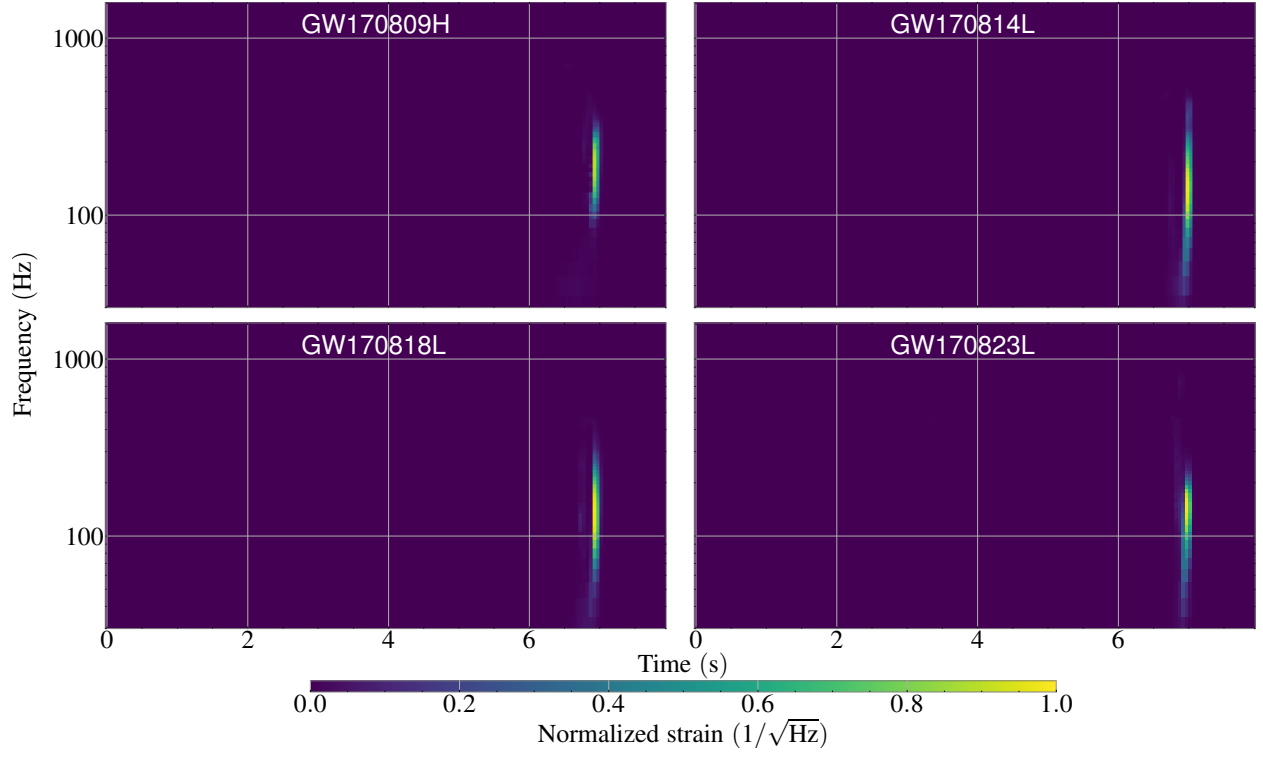


FIG. 11: Same as Fig. 7, but for the remaining time-frequency representation of GW events from GW170809 to GW170823.

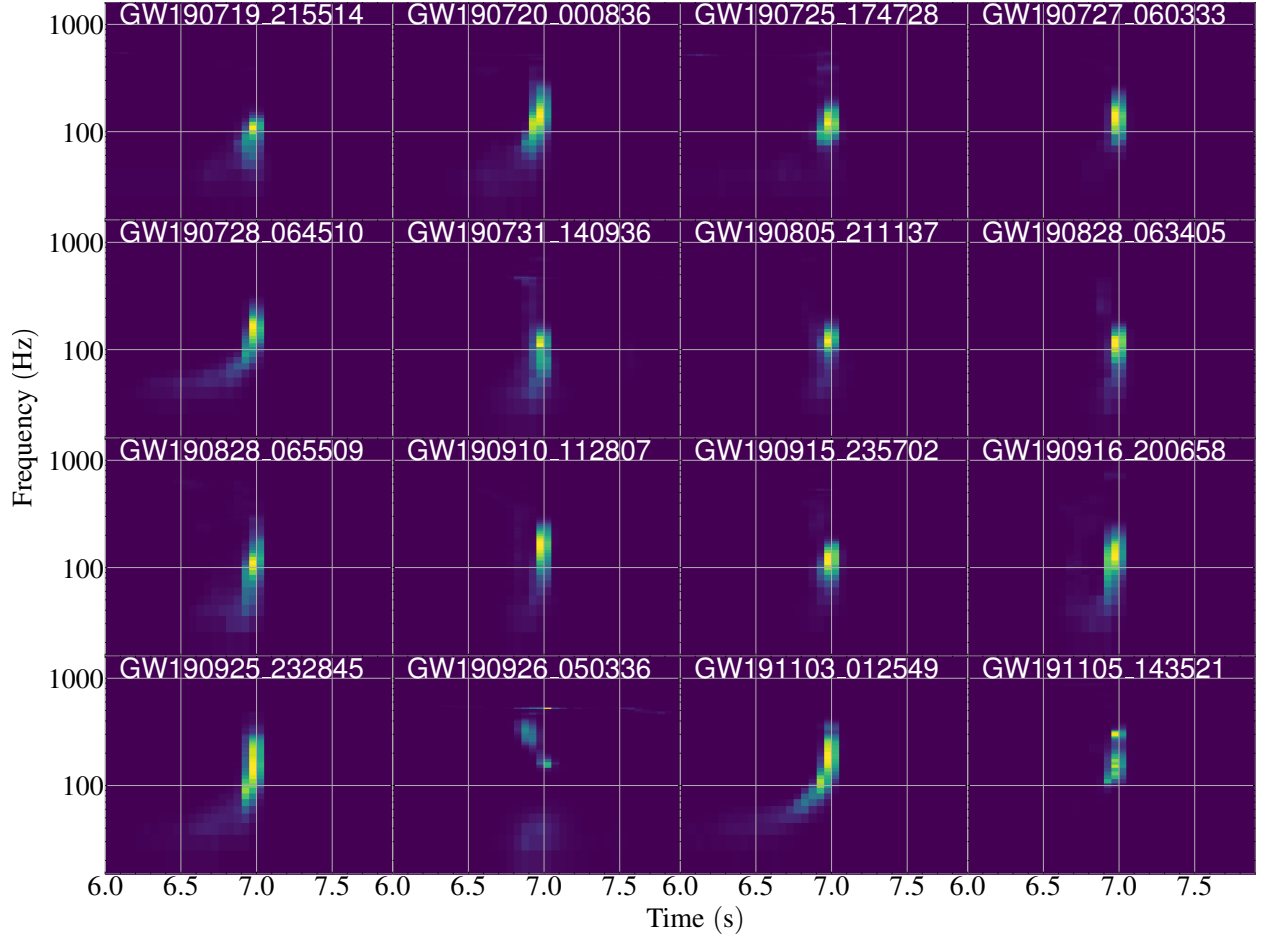


FIG. 12: Same as Fig. 8, but for the remaining time-frequency representation of GW events from GW190719.215514 to GW191105.143521.

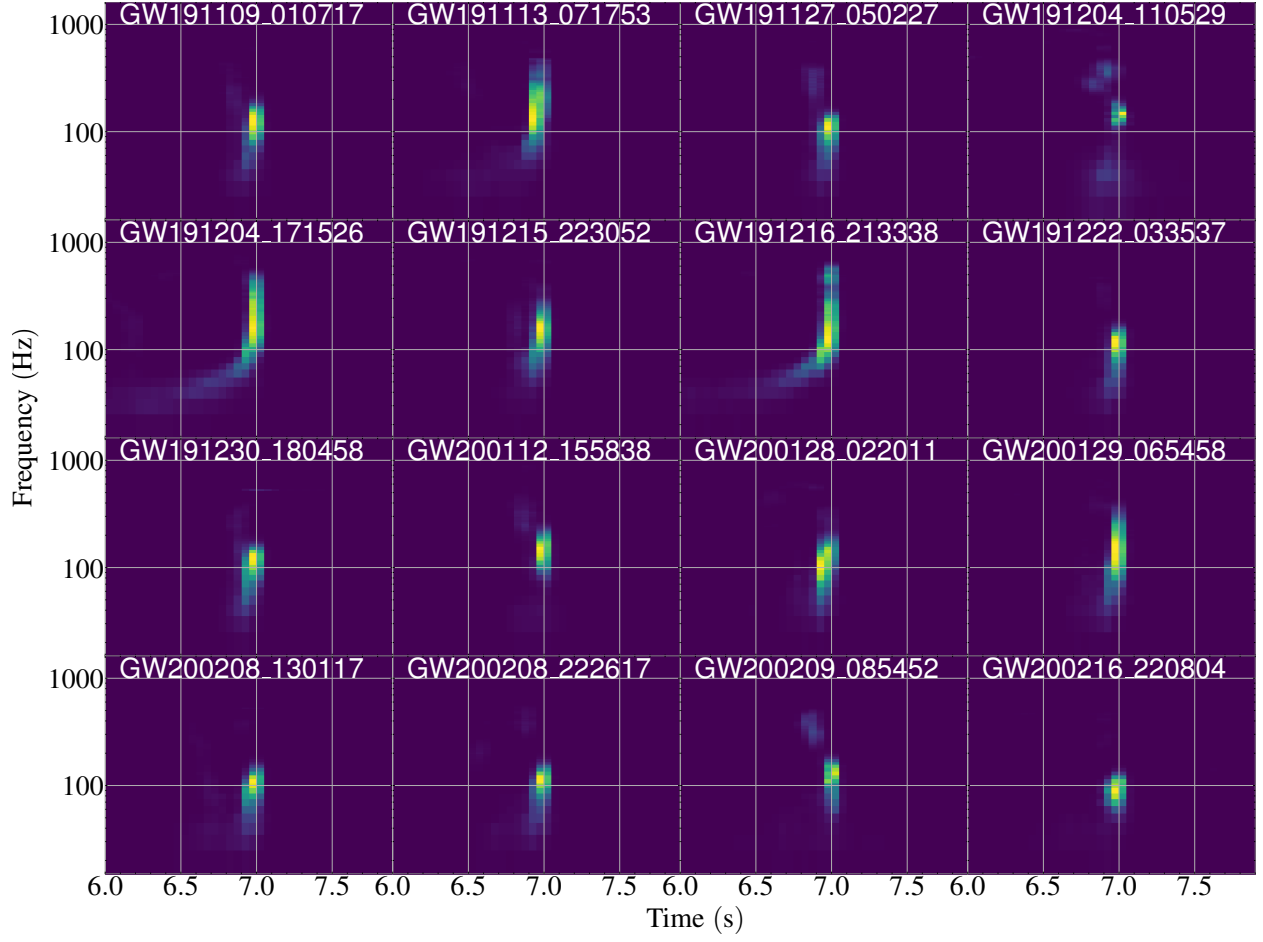


FIG. 13: Same as Fig. 8, but for the remaining time-frequency representation of GW events from GW191109.010717 to GW200216.220804.

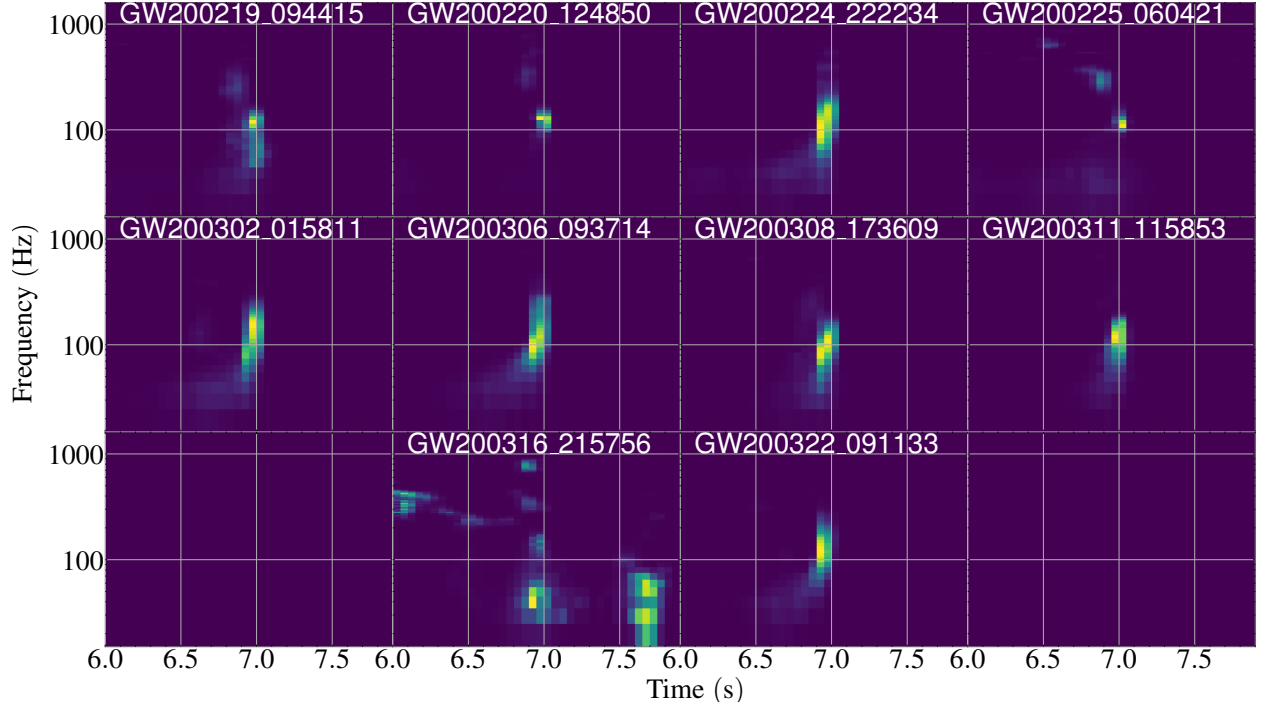


FIG. 14: Same as Fig. 8, but for the remaining time-frequency representation of GW events from GW200219_094415 to GW200322_091133.